Molecular-dynamics simulations of the thermal glass transition in polymer melts: α-relaxation behavior

Christoph Bennemann, Wolfgang Paul, and Kurt Binder
Institut für Physik, 55099 Mainz, Germany

Burkhard Dünweg
MPI für Polymerforschung, Ackermannweg 10, 55128 Mainz, Germany

(Received 11 August 1997)

We present molecular-dynamics simulations of the thermal glass transition in a dense model polymer liquid. We performed a comparative study of both constant volume and constant pressure cooling of the polymer melt. Great emphasis was laid on a careful equilibration of the dense polymer melt at all studied temperatures. Our model introduces competing length scales in the interaction to prevent any crystallization tendency. In this first manuscript we analyze the structural properties as a function of temperature and the long time or α-relaxation behavior as observed in the dynamic structure factor and the self-diffusion of the polymer chains. The α relaxation can be consistently analyzed in terms of the mode coupling theory of the glass transition. The mode coupling critical temperature T_c, and the exponent γ defining the power law divergence of the α-relaxation time scale, both depend on the thermodynamic ensemble employed in the simulation.
[S1063-651X(98)07101-3]

PACS number(s): 64.70.Pf, 61.25.−f, 83.10.Nn

I. INTRODUCTION

Understanding the glass transition in supercooled materials is a great challenge in condensed matter theory [1,2] and also of high technological importance [3]. Polymers constitute a class of materials with a very small crystallization tendency. The ubiquity of amorphous polymeric materials has made them a longstanding focus of the experimental characterization of the glass transition [4] and of efforts to derive models of this transition [5]. Traditionally this work focused on the temperature range in which the typical relaxation times in the material are macroscopic, i.e., in the range of seconds.

With the development of the mode coupling theory (MCT) of the glass transition [2,6–9], interest was shifted to the temperature regime of the supercooled liquid and relaxation times in the ns–μs range. This ignited a tremendous effort over the last decade [10–12] on the side of experiment and computer simulations to test the predictions and range of validity of this theory on all kinds of glass forming materials. Originally this theory was developed for hard sphere liquids, but it has been applied to and claimed to have been tested on as diverse materials such as colloids [13,14], ionic glasses [15], molecular liquids [16], and polymers [17]. The emerging picture seems to be that the theory can be applied in situations where the glass transition is determined by the repulsive part of the intermolecular interactions, i.e., where there are no site specific attractive interactions which could give rise, for instance, to network formation like in SiO_2.

On the computer simulation side, there has been a very detailed test of MCT on a mixture of Lennard-Jones particles [18–20], which belongs to the class of materials discussed above. The glass transition in polymer melts has been studied in great detail with Monte Carlo simulations of the bond fluctuation model [21–27], which can also be applied to the modeling of real polymers [28]. The combination of lattice model and Monte Carlo methods necessarily means that in general one studies the glass transition at a constant volume, and that one completely neglects inertia effects in the short time dynamics. Any motions on scales smaller than a lattice spacing are completely eliminated, of course. Both of these drawbacks can be remedied by resorting to a molecular-dynamics simulation of a continuum model. Work in this direction mainly used atomistic polyethylenelike models. Early work [29,30] focused on the glass transition as a phenomenon of macroscopic time scales, observing the break in the dependence of the specific volume on temperature. This study, as well as later work [31,32], used high quenching rates, losing one of the main advantages of such polymeric glass formers, namely, the ability to equilibrate chain conformations and local packing in the amorphous state without intervening crystallization tendencies. In the series of works [30–32], no systematic study of quenching rate effects or the degree of equilibration at different temperatures was reported on. In particular, for the dynamic structure factor, it has been shown [22,23] that the observed behavior depends strongly on the degree of equilibration one has achieved.

Thus we decided to perform a systematic study of the glass transition in a polymer melt using a simple coarse-grained polymer model in the continuum consisting of Lennard-Jones particles connected by nonlinear springs [33]. This model can be equilibrated with respect to local packing and chain conformations down to temperatures well in the regime of the supercooled liquid. All our results on the dynamic properties of the polymer melt are therefore equilibrium dynamics. We also decided to simulate this model under constant volume (NVT) as well as constant pressure (NpT) conditions to study the difference and similarities of the glass transition in these ensembles. Since both cooling methods follow different paths in the state space of the model, we expect quantitative differences between the observations at constant volume and constant pressure, albeit

qualitatively similar behavior, as was seen experimentally [34]. For a direct quantitative comparison one would need, for instance, a whole set of constant pressure cooling curves.

The remainder of this paper is organized as follows. In Sec. II, we will discuss our model and the simulation procedure for the NVT as well as NpT simulations. Section III will present a comparison of the static properties of the melts in the NVT and NpT simulations. In Sec. IV, we will discuss our results for the α-relaxation dynamics as observed in the dynamic structure factor and the self-diffusion of the polymer chains. Section V will present our conclusions. A detailed analysis of the β-relaxation regime predicted by mode coupling theory along the lines of Refs. [22,23] will be presented in a forthcoming work.

II. MODEL AND SIMULATION TECHNIQUE

For modeling the intermolecular and intramolecular forces, we used a bead-spring model derived from the one suggested by Kremer and Grest [33], and also used in several recent simulations [35,36]. However, here we also included the attractive part of the Lennard-Jones potential, since previous work [24,25] had showed that without such an attraction the model would produce a negative thermal expansion coefficient.

Each chain consisted of ten beads with mass m set to unity. Between all monomers there acted a truncated Lennard-Jones potential

$$U_{\mathrm{LJ}}(r_{ij})=\begin{cases} 4\epsilon\left[\left(\dfrac{\sigma}{r_{ij}}\right)^{12}-\left(\dfrac{\sigma}{r_{ij}}\right)^{6}\right]+C: & r_{ij}<2\times 2^{1/6}\sigma \\ 0: & r_{ij}\geqslant 2\times 2^{1/6}\sigma, \end{cases} \tag{1}$$

where C was a constant which guaranteed that the potential was continuous everywhere. Since it was not our aim to simulate a specific polymer, we used Lennard-Jones units where ϵ and σ are set to unity. Note that this means that all quantities are dimensionless. In addition to the Lennard-Jones potential, a finitely extendable nonlinear elastic (FENE) backbone potential was applied along the chain

$$U_F(r_{ij})=-\frac{k}{2}R_0^2\,\ln\left[1-\left(\frac{r_{ij}}{R_0}\right)^2\right]. \tag{2}$$

The parameters of the potential were set to $k=30$ and $R_0=1.5$, guaranteeing a certain stiffness of the bonds while avoiding high frequency modes (which would require a rather small time step for the integration) and chain crossing. Furthermore, with these parameters we set the favored bond length to a value slightly lower than the length favored by the Lennard-Jones potential. Thus we introduced two different incompatible length scales in our system, which should help to prevent the emergence of long range order at lower temperatures.

All simulations in the NVT ensemble were performed using a Nosé-Hoover thermostat [37,38] to keep the temperature at the desired level. In this technique the model system is coupled to a heat bath which represents an additional degree of freedom represented by the variable ζ. The equations of motion are

$$\frac{d\mathbf{q}_i}{dt}=\frac{\mathbf{p}_i}{m_i}, \tag{3}$$

$$\frac{d\mathbf{p}_i}{dt}=\mathbf{F}_i-\zeta\mathbf{p}_i, \tag{4}$$

$$\frac{d\zeta}{dt}=\frac{1}{Q}\left(\sum_i \frac{\mathbf{p}_i^2}{m_i}-gk_BT\right), \tag{5}$$

where $\mathbf{F}_i$ is the total force acting on particle i due to the potentials described above, and Q represents the mass of the heat bath, while g is the number of degrees of freedom. Note that ζ fluctuates around zero, and can thus become negative. The mass Q has to be chosen with great care [39,40], since otherwise one may not obtain a canonical distribution. If, for example, Q is very large, the kinetic energy and therefore the temperature starts to oscillate with an undesired large amplitude. Instead of a canonical distribution one then obtains a two-peaked distribution. In principle, any problems could be avoided by using a chain of thermostats [41], but that would have worsened the computational effort and was thus discarded. For optimal results the intrinsic frequency of the heat bath should be approximately equal to the intrinsic frequency of the model system, a theoretical estimate of which was obtained by calculating the frequency of a particle in a fcc lattice subjected to Lennard-Jones potentials. The intrinsic frequency of the heat bath is given by [40]

$$\frac{1}{\omega_s}=2\pi\sqrt{\frac{Q}{2gk_BT}}. \tag{6}$$

Setting ω_s equal to the theoretically obtained frequency, and rearranging this equation, yields an expression for Q. Note that Q depends explicitly on the temperature, and therefore had to be adjusted for every simulation temperature. During all simulations no suspicious behavior due to the choice of Q was observed. We also performed several Monte Carlo (MC) simulations using both a continuum configurational bias method [42,43] and so-called smart reptation which were carried out at the temperature $T=1.0$ in order to check the validity of the molecular-dynamics (MD) algorithm and to investigate whether this could be a potentially faster means for obtaining equilibrated configurations. For the dense melts we studied we found, however, that the fastest way to equilibrate the system was to use our standard MD algorithm. The measured static properties, as obtained in the MC simulations, were in good agreement with the measured static properties of the configurations produced with the molecular-dynamics algorithm. Furthermore, the obtained energy distributions were similar. To check what influence the Nosé-Hoover thermostat has on the Newtonian dynamics, we also carried out some simulations in the microcanonical ensemble, and compared the results to the results of the simulations with Nosé-Hoover thermostat. Both methods lead to the same results; for example, the velocity autocorrelation function of the two simulations were identical (Fig. 1). This means that the thermostat only has a weak influence on the Newtonian dynamics, although one is able to tune the temperature with it very effectively.

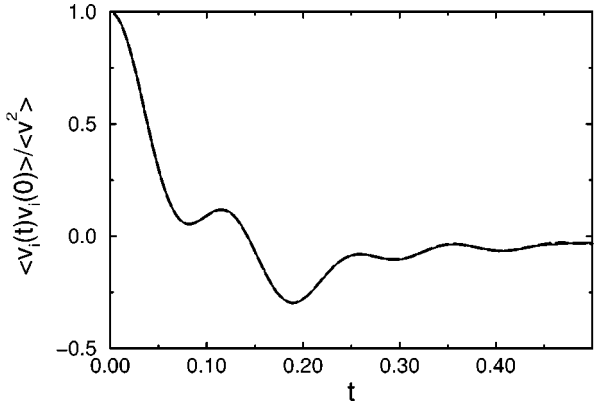

FIG. 1. Velocity autocorrelation function with and without a (dashed line) Nosé-Hoover thermostat. The two lines are practically identical, meaning that the thermostat has only a weak influence on the Newtonian dynamics. Note that because we were using Lennard-Jones units, all quantities shown are dimensionless.

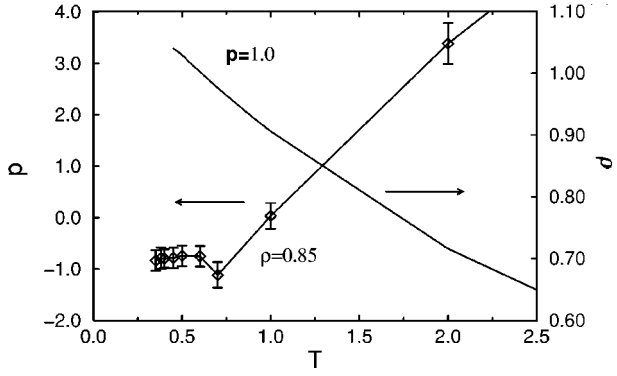

FIG. 2. Thermodynamic paths for the cooling experiments we performed in the simulation.

Starting configurations were obtained using the method proposed by Kremer and Grest [33,36]. Before being subjected to the Nosé-Hoover thermostat, each configuration thus generated was propagated in the microcanonical ensemble ($Q=\infty$). At the beginning of this step the velocities were rescaled several times in order to come close to the desired temperature range. In the next equilibration step the thermostat was switched on, and the system was propagated until the mean square displacement of the centers of mass of the polymer chains had reached several R_g^2, R_g denoting the radius of gyration. At this time all measured correlators had already decayed to zero.

In order to speed up computational efficiency, we applied a linked cell scheme combined with a Verlet table [44]. Because of the Nosé-Hoover thermostat it was not possible to use a velocity Verlet algorithm; instead we used a Heun algorithm [45] with a time step of $dt=0.002$.

All simulations in the NVT ensemble were performed using 95 polymer chains, each consisting of ten monomers. The volume was held constant at $V=1117.65$ ($\rho=0.85$). Since the density was the same for all temperatures, it was not necessary to generate starting configurations at every temperature, as it was for the simulations in the NpT ensemble, but one could use the ones generated and equilibrated at another temperature and equilibrate them again at the new temperature. Simulations were performed at temperatures $T=0.35$, 0.38, 0.4, 0.45, 0.5, 0.6, 0.7, 1.0, and 2.0. For statistical reasons ten different configurations were simulated at each temperature. The equilibration of a configuration at the lowest temperature required 30×10^6 MD steps, or almost two weeks of CPU time on an IBM Power PC for each configuration.

Since in the simulations of the NpT ensemble we wanted to keep the average pressure at $p=1.0$ at all temperatures, the situation differed from the one of the simulation of the NVT ensemble. In a first step we used a MD algorithm, which also allowed for volume fluctuations of the system [39,46], to obtain the average density of the system at a certain temperature. These runs lasted up to 5×10^6 MD steps. Afterwards, in a procedure analogous to the one described above, we used the found density to generate starting configurations which we used for NVT simulations. Note that we performed the simulations themselves at constant volume, but this procedure made sure that the average pressure was constant (within 5%) at all temperatures. This was done because NVT simulations are computationally more efficient, and also because we observed better stability for NVT than for NpT simulations. At almost all temperatures we simulated 120 polymer chains, each consisting of ten monomers. Furthermore, at each temperature ten different configurations were simulated, and simulations were performed at temperatures $T=0.48$, 0.5, 0.52, 0.55, 0.6, 0.65, 0.7, 1.0, and 2.0.

III. STATIC PROPERTIES

In this section we will discuss the static properties of the melts as a function of temperature. The thermodynamic paths for our cooling processes in the NVT and NpT ensembles are shown in Fig. 2. In the NVT ensemble we started our simulation at modestly high pressure at a high temperature. Upon cooling, the pressure decreases, and becomes negative around $T=0.7$. This negative pressure has consequences which we will discuss in detail when analyzing the structure factor of the melt. In the NpT ensemble we keep the pressure at an ambient value, and adjust the density upon cooling.

A. Chain conformations

Let us now first look at the chain conformations upon cooling. The Hamiltonian we chose has no intramolecular bond angle part, and therefore there is no tendency of our chains to become stiffer at lower temperatures. Consequently the size of the chains varies very little in our whole temperature range ($R_g=2.10$ at $T=0.35$, and $R_g=2.23$ at $T=2.0$ in the NVT ensemble, and $R_g=2.09$ at $T=0.48$, and $R_g=2.23$ at $T=2.0$ in the NpT ensemble). In Fig. 3 we show the behavior of the structure factor of the chains in the NVT ensemble for the lowest simulation temperature. Also included is a Debye function [47] calculated with the independently measured radius of gyration. The good agreement with the simulation data shows that the chains remain Gaussian on the large scale over the whole temperature range. The stiffness parameter C_N was in the range of 1.51 to 1.56.

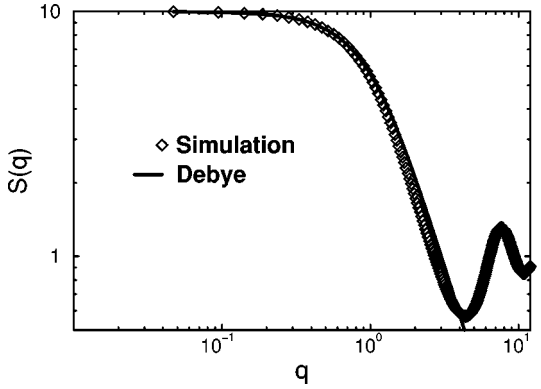

FIG. 3. Structure factor of the chains for the lowest simulation temperature. Also shown is the Debye function corresponding to the independently measured radius of gyration.

B. Packing behavior

The effect of the two competing length scales we introduced into our model can be nicely seen by looking at the monomer-monomer pair correlation function shown in Fig. 4. First of all we want to note that the pair correlation function shows no long-range ordering even at the lowest temperature we studied. The nearest neighbor peak, which is just a diffuse peak around $r=1.0$ at high temperatures, splits in two upon cooling. The first of the peaks is due to the preferred intramolecular distance or bond length $b=0.96$. The second peak is the preferred nearest neighbor position in the minimum of the intermolecular Lennard-Jones interaction at $r_{\min}=2^{1/6}$.

For the NVT ensemble this real space behavior transforms into the structure factor of the melt shown in Fig. 5. The amorphous structure is manifest here in the amorphous halo around $q=6.9$, which contains both intramolecular and intermolecular nearest neighbor contributions. With decreasing temperature the short-range intermolecular order increases, and since this is the larger of the two length scales contributing to the amorphous halo, its position shifts to smaller q values at first. At lower temperatures, however, this shift is reversed, and the peak moves to higher q values, as would be expected for thermal contraction of the sample. In the same temperature range a small peak at very small q values ($q\approx1.7$) develops. Both effects result from a microvoid developing in the system, because we are in a range of negative

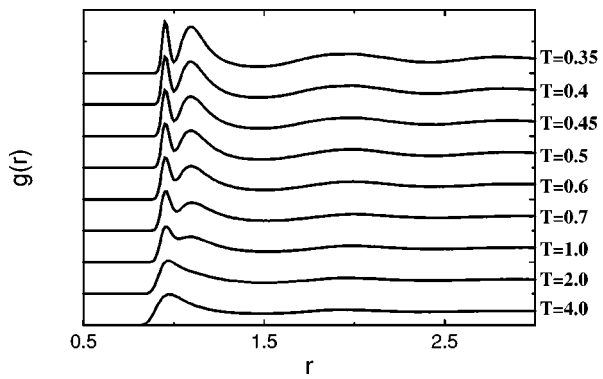

FIG. 4. Pair correlation function for the NVT simulations and the range of indicated temperatures. Curves for lower temperatures are shifted upward.

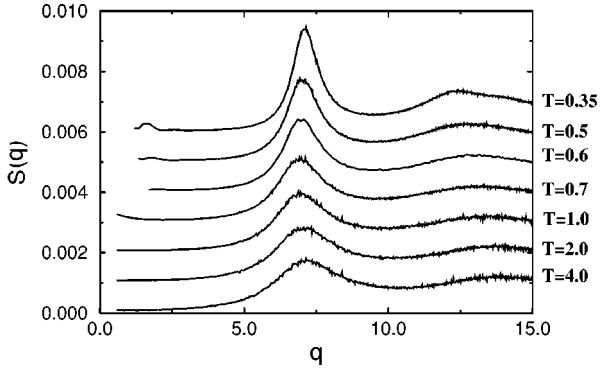

FIG. 5. Structure factor of the melt for a set of temperatures in the NVT simulations. Note the appearance of a small peak at low q values around $T=0.6$, which is due to the emergence of a microvoid in the system.

pressure where the system would be likely to contract into a dense melt, expelling the free volume. The microvoid, which contains up to around 5% of the simulation volume, can be identified both by visual inspection and numerical analysis. The position of the small q peak is related to the typical diameter of a microvoid. For the NVT simulations, we therefore have to keep in mind that at the lowest temperatures our system is no longer homogeneous but contains a small amount of internal surfaces.

For the NpT simulations this effect is of course absent, as can be seen in Fig 6. In this case the structure factor shows the behavior also seen experimentally, with the amorphous halo moving to larger q values due to the increased density at lower temperatures.

IV. DYNAMIC PROPERTIES

In this section we will look at the temperature dependence of the largest relaxation time in the melt. For simple glass forming liquids this is called the α-relaxation time. This is the time scale at which a particle breaks free of the cage of its nearest neighbors, and large scale structural relaxation becomes possible. For polymers then, this also is the time scale on which local conformational rearrangements start to occur. The largest relaxation time in polymers, however, is the time for the overall renewal of the chain conformation, which is a factor of N^2 (N being the number of monomers in a polymer chain) larger for chains following Rouse dynamics [48], and a factor of N^3 for larger chains where reptation

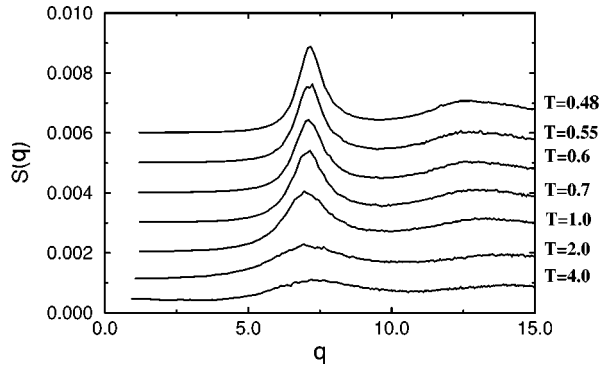

FIG. 6. Same as Fig. 5 for the NpT simulations.

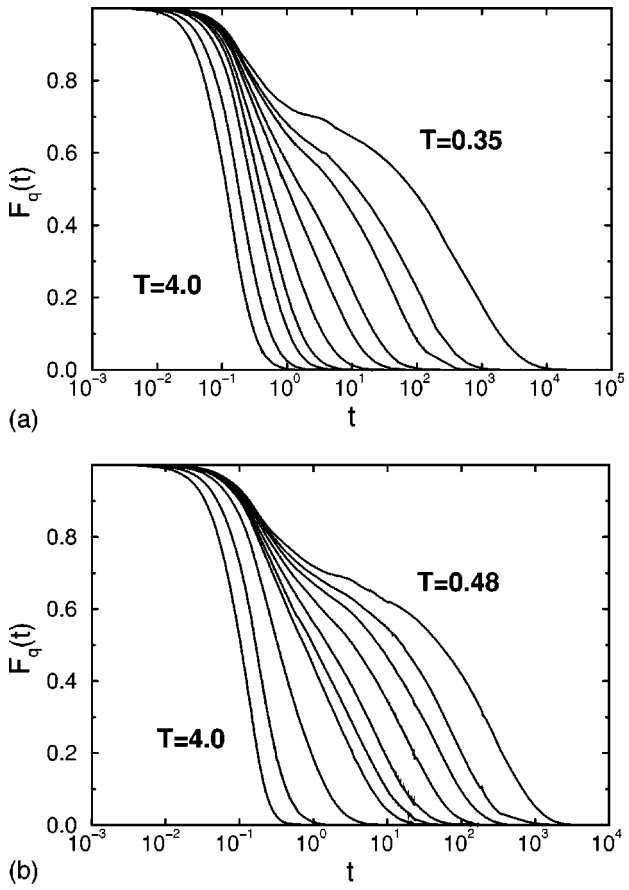

FIG. 7. Intermediate dynamic structure factor at the first maximum of the static structure factor for the NVT simulations (a) and the same for the NpT simulations (b).

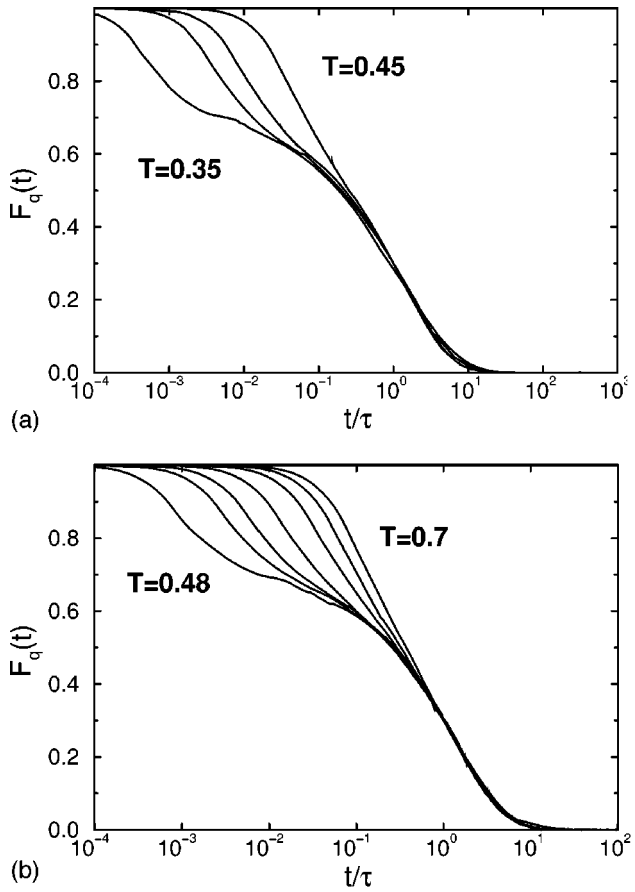

FIG. 8. Same as Fig. 7, but with times scaled by the α-relaxation time scale for the range of temperatures where the time-temperature superposition holds. (a) NVT ensemble. (b) NpT ensemble.

effects have to be taken into account [47]. The temperature dependence of this longest relaxation time is determined by the temperature dependence of the prefactor in these scaling laws, which is the time scale for local conformational changes, which, as discussed, is enslaved to the α process of the structural relaxation.

A. Structural relaxation

We will discuss the structural relaxation in terms of the incoherent intermediate dynamic structure factor

$$F_q(t)=\left\langle \frac{1}{M}\sum_{i=1}^{M} e^{i\mathbf{q}\cdot[\mathbf{r}_i(t)-\mathbf{r}_i(0)]}\right\rangle, \tag{7}$$

where M stands for the total number of monomers in the melt. As can be seen in Fig. 7, which shows $F_q(t)$ at the peak position of the static structure factor, the intermediate dynamic structure factor starts to exhibit a two step relaxation process when lowering the temperature, the so-called β and α processes. In this paper we focus on the behavior of the long-time α process, and leave a detailed analysis of the β relaxation to a forthcoming publication.

Comparing the behavior of the NVT [Fig. 7(a)] and NpT simulations [Fig. 7(b)], we see that the slowing down of the structural relaxation and the development of the two step process occur for higher temperatures in the NpT ensemble. The behavior of $F_q(t)$ at the first minimum of the static structure factor is qualitatively the same, with the plateau region occurring at a smaller value of $F_q(t)$. We empirically define an α-relaxation time scale by the requirement

$$F_q(\tau_\alpha)=0.3. \tag{8}$$

In the undercooled liquid close to the mode coupling critical temperature the time-temperature superposition principle is expected to hold. Figures 8(a) and 8(b) show that indeed we find a superposition of the α-relaxation behavior for the NVT simulation in the region $0.35<T<0.45$; for the NpT simulations this occurs in the range $0.48<T<0.6$.

One generally also analyzes the α-relaxation behavior by fitting the empirical Kohlrausch-Williams-Watts formula to the data,

$$f(t)=Ae^{-(t/\tau)^{\beta}}. \tag{9}$$

In the temperature range where we found the time-temperature superposition principle to hold, we find

$$\beta=0.56\pm0.04 \ \text{(NVT)}; \quad \beta=0.7\pm0.08 \ \text{(NpT)}. \tag{10}$$

The error bars are mostly due to the effect that one can change β by almost 15% by changing the time interval over which one tries to fit the data. When one tries to fit the behavior at higher temperatures, the resulting values for β increase, approaching unity at high temperatures.

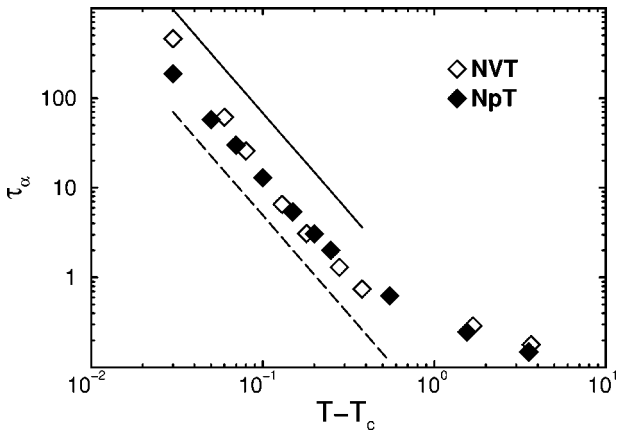

FIG. 9. Critical behavior of the α-relaxation time scale close to the respective critical temperatures, $T_c=0.32$ in the NVT ensemble and $T_c=0.45$ in the NpT ensemble, plotted against $T-T_c$. Open diamonds are for the NVT ensemble, and closed diamonds are for the NpT ensemble.

For the α-relaxation time scale the mode coupling theory of the glass transition predicts a power law divergence

$$\tau_\alpha \propto (T-T_c)^{-\gamma}. \tag{11}$$

Figure 9 shows that we indeed observe this behavior with T_c and γ depending on the thermodynamic ensemble. For the NVT simulations we obtain $T_c=0.32\pm0.01$ and $\gamma=2.3\pm0.2$, and for the NpT simulations we have $T_c=0.45\pm0.01$ and $\gamma=1.95\pm0.15$. For our model we therefore equilibrated our system to temperatures within 10% of T_c. Note that near T_c in the NpT ensemble the density is much higher than for our choice of density in the NVT ensemble, and thus the large difference of T_c is not unexpected.

However, it should be mentioned that it is in principle also possible to fit our data with the well-known Vogel-Fulcher-Tammann (VFT) equation

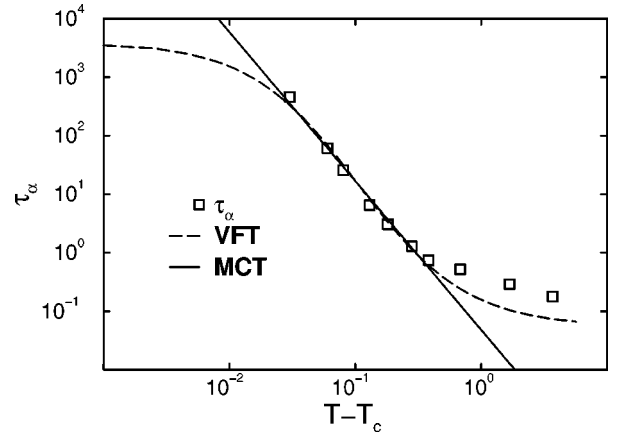

FIG. 10. τ_α as measured in the NVT ensemble. Also shown are best fits with the VFT equation, and the predictions of MCT. The temperature range is shifted by $T_c=0.32$ to show the similarity of the predictions of the two equations for our data close to T_c. Note that very similar plots can be obtained for the quantities discussed in Fig. 12.

$$\tau_\alpha = \tau_0 \exp\left(\frac{E}{T-T_0}\right). \tag{12}$$

As can be seen in Fig. 10, we obtain $T_0=0.215\pm0.02$ and $E=1.1\pm0.1$ for the NVT simulations, and $T_0=0.34\pm0.02$ and $E=0.93\pm0.1$ for the NpT simulations. Close to the mode coupling critical temperature the VFT curve is well approximated by a power law divergence with exactly the same critical temperature and exponent as obtained from an independent mode coupling fit. Very close to T_c the VFT curve flattens in comparison with the ideal mode coupling fit. This is again in accord with what would be predicted by an extended mode coupling analysis [22], taking into account structural decay via activated processes. It is also a behavior typically seen in experiment [49] and simulations [50].

B. Polymer self-diffusion

The overall conformational relaxation of polymer molecules can be conveniently analyzed by looking at their self-diffusion behavior [51]. For this purpose one can look at

$$g_1(t)=\langle[\mathbf{r}^j_{N/2}(t)-\mathbf{r}^j_{N/2}(0)]^2\rangle, \tag{13}$$

which describes the mean square displacement of the inner monomers (j labels different polymer chains). The analogous quantity in the center-of-mass reference frame of chain j [$\mathbf{r}^j_{cm}(t)$ being the position of the center of mass of polymer j at time t] is

$$g_2(t)=\langle[\mathbf{r}^j_{N/2}(t)-\mathbf{r}^j_{\rm cm}(t)-\mathbf{r}^j_{N/2}(0)+\mathbf{r}^j_{\rm cm}(0)]^2\rangle. \tag{14}$$

The mean square displacement of the center of mass itself is

$$g_3(t)=\langle[\mathbf{r}^j_{\rm cm}(t)-\mathbf{r}^j_{\rm cm}(0)]^2\rangle. \tag{15}$$

Finally, the mean square displacement of monomers at the free ends of the chains, and the analogous quantity in the center-of-mass reference frame, are defined as

$$g_4(t)=\langle[\mathbf{r}^j_{\rm end}(t)-\mathbf{r}^j_{\rm end}(0)]^2\rangle \tag{16}$$

$$g_5(t)=\langle[\mathbf{r}^j_{\rm end}(t)-\mathbf{r}^j_{\rm cm}(t)-\mathbf{r}^j_{\rm end}(0)+\mathbf{r}^j_{\rm cm}(0)]^2\rangle. \tag{17}$$

Figure 11(a) shows g_1 to g_5 measured at $T=1.0$, and Fig. 11(b) the same quantities at $T=0.35$ as measured in the NVT ensemble. For $g_1(t)$ one can distinguish several regimes. For short times $t<0.1$ one observes a ballistic regime which is followed by a subdiffusive regime and finally a free diffusion regime. Such a behavior is typical of polymer systems, and is predicted by many theories, e.g., the Rouse model. As can be seen in Fig. 11(b), the situation is a little bit different at lower temperatures. The ballistic regime is now followed by a plateaulike regime which precedes the subdiffusive one. Such a plateau regime is typical for glass formers, and a sign of the onset of the structural arrest of the system. The height of the plateau is closely related to the size of the cage a particle is trapped in. Another difference from high temperatures is that the subdiffusive regime stretches out far more in time and, therefore, the free diffusion limit is reached only after long simulation times.

The subdiffusive regime can be fitted using

$$g_1(t)=\sigma^2(W_1 t)^{x_1}. \tag{18}$$

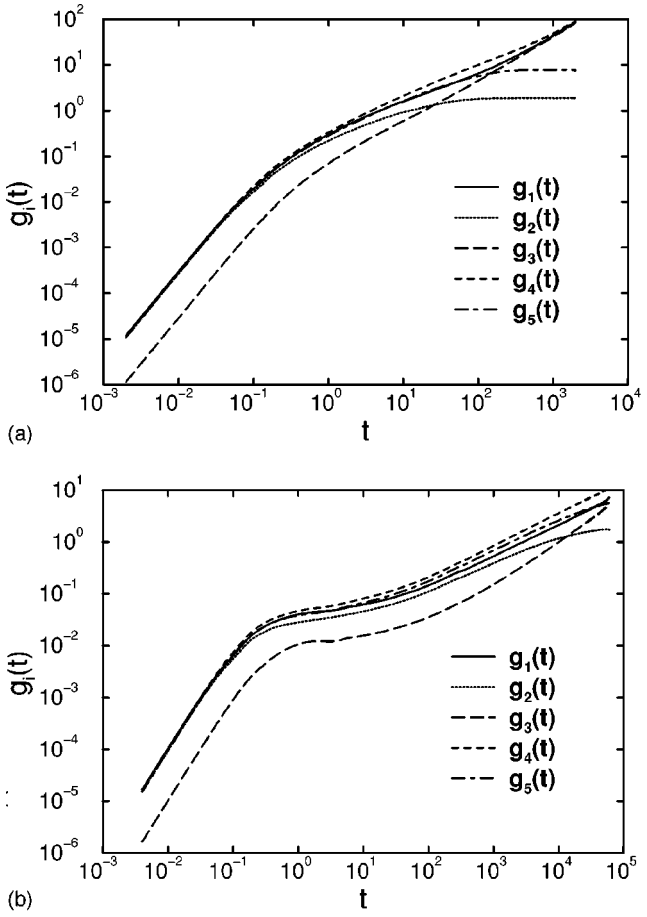

FIG. 11. Mean square displacements as a function of time for $T=1.0$ (a) and $T=0.35$ (b). g_3 describes the center of mass of the chain, g_1 and g_4 are center and end monomers, respectively, and g_2 and g_5 are the corresponding displacements in the center-of-mass reference frame. All quantities shown were measured in the NVT ensemble.

We obtain $x_1=0.62\pm0.02$ for all simulated temperatures. $g_4(t)$ behaves similarly to $g_1(t)$. Here the diffusive regime is preceded by a subdiffusive one as well, which can be fitted by

$$g_4(t)=\sigma^2(W_4t)^{x_4}. \tag{19}$$

Again the exponent is approximately the same at all temperatures. We find $x_4=0.67\pm0.03$.

If our model chains would exactly follow the Rouse predictions, the local monomer mobilities W_1 and W_4 should be equal, and x_1 and x_4 should be equal to 0.5. It is, however, a general finding from simulations that, for chains as short as ours, one generally observes a smeared out crossover behavior [21] from short- to long-time diffusion instead of the predicted Rouse exponent. At later times, $g_1(t)$, $g_3(t)$, and $g_4(t)$ all show the expected simple diffusive behavior

$$g_i(t)=6Dt, \tag{20}$$

where the self-diffusion constant is the same for all i. At lower temperatures, especially for $g_1(t)$ and $g_4(t)$, it is very hard to distinguish this regime from the preceding subdiffusive one.

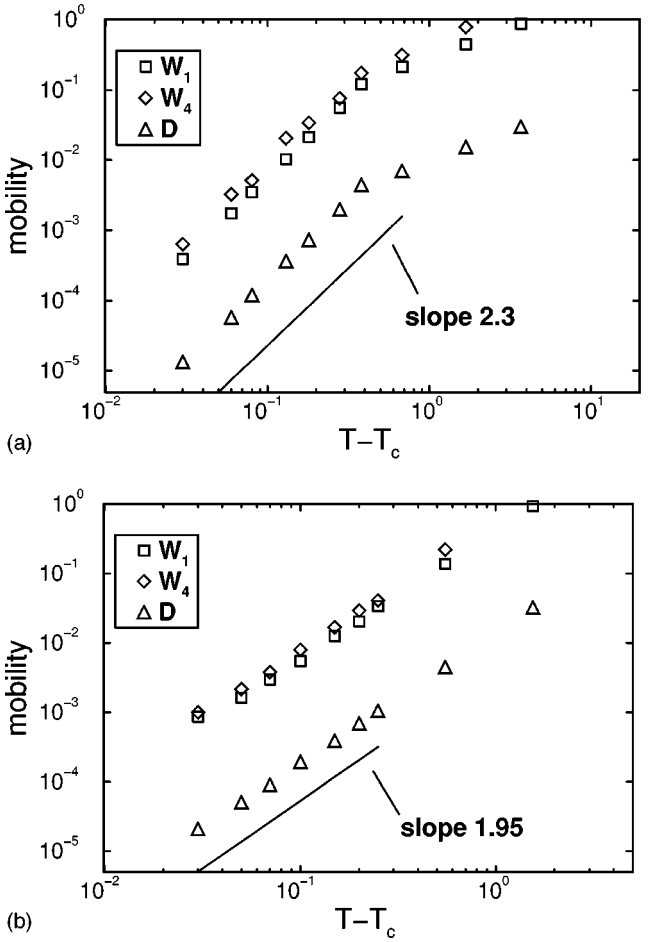

FIG. 12. Critical behavior of the self-diffusion coefficient and the rate constants for the NVT (a) and NpT simulations (b).

In Fig. 12, $D(T)$, $W_1(T)$, and $W_4(T)$ are plotted against the temperature. As one sees for lower temperatures, all quantities follow a power law behavior

$$D\propto(T-T_c)^{\gamma}, \tag{21}$$

$$W_i\propto(T-T_c)^{\gamma}, \quad i=1,4. \tag{22}$$

The critical temperature and the exponent are, within a range of error, the same as those for the α-relaxation time scale in the respective ensemble. This shows the coupling of the conformational relaxation and diffusion of the polymer chains to the local structural α relaxation in the melt, as discussed in the beginning of this section. Note that it is again possible to fit the data with the VFT equation using the same T_0 and E (within the range of error) as obtained when fitting the α-relaxation times.

V. CONCLUSIONS

In this paper we have presented a molecular-dynamics simulation of the thermal glass transition in dense polymer melts. We have studied this transition at constant density as well as constant pressure. Our model is a coarse-grained bead-spring model with nonlinear springs connecting monomers along a chain and Lennard-Jones interactions between all monomers. In order to introduce packing frustration into the model, we chose incompatible length scales for intra-

molecular and intermolecular nearest neighbor distances. All our results were obtained on well equilibrated samples.

We showed that the static structure factor of our chains of length $N=10$ could be well described by a Debye function at all temperatures. The size of the chains is mostly temperature independent, as we introduced no temperature dependent stiffness into the model. The two incompatible length scales in the Hamiltonian can be seen in a split of the first neighbor peak of the monomer-monomer pair correlation function at low temperatures. For the constant volume simulation, the density we chose led to negative pressure for $T<0.7$. This instability led to the buildup of microvoids taking up approximately 5% of the simulation volume at low temperatures. The observed negative pressure is an indication that the void formation process is not fully completed on the time scale of the simulation.

In this work we analyzed the glass transition in terms of the α-relaxation process. The divergence of the α-relaxation time scale could be very well described by the power law behavior predicted by MCT. Critical temperatures differ substantially, and power law exponents differ slightly between cooling at constant volume and cooling at constant pressure. The divergence of the α-relaxation time scale also leads to a divergence of the largest relaxation time in the system, which is the Rouse time for the overall renewal of the chain conformations. This divergence can be observed by looking at the mobility of monomers on intermediate length scales (as measured by the rate constants W_1 and W_4) and the center of mass self-diffusion coefficient of the chains. All these quantities follow power law singularities with values for the critical temperatures and exponents in nice agreement with the behavior of the α-relaxation time scale. The divergence could be equally well described by a VFT fit to the data, and it could be shown that close to T_c the MCT power law singularity is a tangent approximation of the VFT curve. A detailed analysis of the β-scaling regime predicted by mode coupling theory of the glass transition will be presented in a separate publication.

ACKNOWLEDGMENTS

We would like to thank J. Baschnagel and W. Kob for helpful discussions, and A. Kopf for supplying his MD code which was modified for the present study. Support by the Sonderforschungsbereich SFB 262, and generous grants of computer time from the computing center of the University of Mainz and the HLRZ Jülich, are gratefully acknowledged.

[1] J. Jäckle, Rep. Prog. Phys. **49**, 171 (1986).
[2] W. Götze and L. Sjögren, J. Phys. C **20**, 879 (1987).
[3] *Material Science and Technology*, edited by J. Zarzycki (VCH, Weinheim, 1991), Vol. 9.
[4] G. B. McKenna, in *Comprehensive Polymer Science*, edited by C. Booth and C. Price (Pergamon, New York, 1989), Vol. 2.
[5] J. H. Gibbs and E. A. DiMarzio, J. Chem. Phys. **28**, 373 (1958).
[6] U. Bengtzelius, W. Götze, and A. Sjölander, J. Phys. C **17**, 59 115 (1984).
[7] W. Götze and L. Sjögren, Rep. Prog. Phys. **55**, 241 (1992).
[8] W. Götze and L. Sjögren, Transp. Theory Stat. Phys. **24**, 801 (1995).
[9] E. Leutheusser, Phys. Rev. A **29**, 2765 (1994).
[10] Proceedings of the 1st International Discussion Meeting on Relaxations in Complex Systems [J. Non-Cryst. Solids **131-133** (1991)], edited by K. L. Ngai, E. Riande, and G. B. Wright.
[11] Proceedings of the 2nd International Discussion Meeting on Relaxations in Complex Systems, edited by K. L. Ngai, E. Riande, and G. B. Wright [J. Non-Cryst. Solids **172-174**, (1994)].
[12] Proceedings of the 3rd International Discussion Meeting on Relaxations in Complex Systems, edited by K. L. Ngai, E. Riande, and G. B. Wright [J. Non-Cryst. Solids (to be published)].
[13] P. N. Pusey and W. van Megen, Nature (London) **320**, 340 (1986); Phys. Rev. Lett. **59**, 2083 (1987).
[14] W. van Megen and S. M. Underwood, Phys. Rev. E **47**, 248 (1993).
[15] F. Mezei, W. Knaak, and B. Farago, Phys. Rev. Lett. **58**, 571 (1987).
[16] E. Roessler and H. Sillescu, in *Material Science and Technology* (Ref. [3]).
[17] B. Frick, B. Farago, and D. Richter, Phys. Rev. Lett. **64**, 2921 (1990).
[18] W. Kob and H. C. Andersen, Phys. Rev. E **51**, 4626 (1995).
[19] W. Kob and H. C. Andersen, Phys. Rev. E **52**, 4134 (1995).
[20] M. Nauroth and W. Kob, Phys. Rev. E **55**, 657 (1997).
[21] W. Paul and J. Baschnagel, in *Monte Carlo and Molecular Dynamics Simulations in Polymer Sciences*, edited by K. Binder (Oxford University Press, Oxford, 1995)
[22] J. Baschnagel and M. Fuchs, J. Phys.: Condens. Matter **7**, 6761 (1995).
[23] J. Baschnagel, Phys. Rev. B **49**, 135 (1994).
[24] M. Wolfgardt, J. Baschnagel, W. Paul, and K. Binder, Phys. Rev. E **54**, 1535 (1996).
[25] M. Wolfgardt and K. Binder, Macromol. Theory Simul. **5**, 699 (1996).
[26] J. Baschnagel, M. Wolfgardt, W. Paul, and K. Binder, J. Res. Natl. Inst. Stand. Technol. **102**, 159 (1997).
[27] K. Okun, M. Wolfgardt, J. Baschnagel, and K. Binder, Macromolecules **30**, 3075 (1997).
[28] W. Paul, K. Binder, K. Kremer, and D. W. Heermann, Macromolecules **24**, 6332 (1991); W. Paul and N. Pistoor, *ibid.* **27**, 1249 (1994); V. Tries, J. Baschnagel, W. Paul, and K. Binder, J. Chem. Phys. **106**, 738 (1997).
[29] D. Brown and J. H. R. Clarke, J. Chem. Phys. **84**, 2858 (1986).
[30] D. Rigby and R.-J. Roe, J. Chem. Phys. **87**, 7285 (1987).
[31] H. Takeuchi, R.-J. Roe, and J. E. Mark, J. Chem. Phys. **93**, 9042 (1990).
[32] R.-J. Roe, J. Chem. Phys. **100**, 1610 (1994).
[33] K. Kremer and G. S. Grest, J. Chem. Phys. **92**, 5057 (1990).
[34] J. Koppelmann, in *Proceedings of the Fourth International*

Congress on Rheology, edited by E. H. Lee and A. L. Copley (Wiley, New York, 1965), Vol. 3.
[35] B. Dünweg, G. S. Grest, and K. Kremer, in *Numerical Methods for Polymeric Systems*, edited by S. G. Whittington (Springer-Verlag, Berlin, in press), Vol. 159.
[36] A. Kopf, B. Dünweg, and W. Paul, J. Chem. Phys. **107**, 6945 (1997).
[37] S. Nosé, Prog. Theor. Phys. Suppl. **103**, 1 (1991).
[38] W. G. Hoover, Phys. Rev. A **31**, 1695 (1985).
[39] W. G. Hoover, Phys. Rev. A **34**, 2499 (1986).
[40] D. Di Tolla und M. Ronchetti, Phys. Rev. E **48**, 1726 (1993).
[41] G. J. Martyna, Michael L. Klein, and Mark Tuckerman, J. Chem. Phys. **97**, 2635 (1992).
[42] J. I. Siepman and D. Frenkel, Mol. Phys. **75**, 59 (1992).
[43] J. J. de Pablo, M. Laso, and U. W. Suter, J. Chem. Phys. **96**, 2395 (1992).
[44] G. S. Grest, B. Dünweg, and K. Kremer, Comput. Phys. Commun. **55**, 269 (1989).
[45] C. W. Gear, *Initial Value Problems in Ordinary Differential Equations* (Prentice-Hall, Englewood Cliffs, NJ, 1970).
[46] S. Melchionna, G. Cicotti, and B. L. Holian, Mol. Phys. **78**, 533 (1993).
[47] M. Doi and S. F. Edwards, *The Theory of Polymer Dynamics* (Clarendon, Oxford, 1986).
[48] P. E. Rouse, J. Chem. Phys. **21**, 1272 (1953).
[49] H. Z. Cummins, G. Li, W. M. Du, and J. Hernandez, Physica A **204**, 169 (1994).
[50] S. Kämmerer, W. Kob, and R. Schilling, Phys. Rev. E **56**, 5450 (1997).
[51] W. Paul, K. Binder, D. W. Heermann, and K. Kremer, J. Chem. Phys. **95**, 7726 (1991).